Unambiguous triplet array beamforming and calibration algorithms to facilitate an environmentally adaptive active sonar concept

Georgios Haralabus
NATO Undersea Research Centre
Viale S. Bartolomeo 400
La Spezia, Italy
Email: haralabus@nurc.nato.int

Alberto Baldacci
NATO Undersea Research Centre
Viale S. Bartolomeo 400
La Spezia, Italy
Email: baldacci@nurc.nato.int

***Abstract*— Cardioid or triplet towed arrays are utilized in sonar applications to resolve left/right ambiguity by placing a null on the ambiguous direction. This leaves an uncalibrated residual signal on the opposite direction from which the desired signal is arriving. Here the mechanism of cardioid beamforming is presented and analytical expressions for the calibration of continuous wave (CW) and linear frequency-modulated (LFM) signals are derived. The validity of these expressions is verified using simulated and real data. The same data sets are also used for comparing the performance between the standard beamformer and a modified version designed to suppress endfire singularities. The effect of correlated vs. uncorrelated intra-triplet noise is assessed using a simulation scenario with a point target.**

I. Introduction

Towed line arrays suffer from port/starboard ambiguity [1], [2] which downgrades active sonar performance. This problem is more evident in the littoral, where strong directional reverberation can mask potential targets on either side of the array [3]. Cardioid or triplet towed arrays were introduced to resolve this problem. They consist of a line of hydrophone triplets made of three closely-spaced omnidirectional hydrophones. Proper combination of the signals from these three hydrophones can make each triplet behave like a single directional hydrophone. Due to the very small distances, intra-triplet noise is usually highly correlated and thus the conventional delay-and-sum beamformer is not relevant. Cardioid beamforming, which is used instead, overcomes this problem by suppressing the signal that arrives from the ambiguous direction, rather than enhancing the one that arrives from the desired direction.

The drawback of cardioid beamforming is that it returns uncalibrated signal levels. This renders the comparison between real and modelled data impossible. Such a comparison is fundamental for the implementation of the environmentally adaptive active sonar concept which was introduced by the NATO Undersea Research Centre (NURC). The proposed adaptation scheme consists of a through-the-sensor environmental assessment, performance predictions via modelling and model validation by means of comparison between real and synthetic data. Based on the outcome of this comparison, the model is then used to provide system feedback on how to improve sonar settings. However, this comparison between modelled and synthetic data is meaningful only if the beamformed signal can be calibrated.

Here mathematical expressions are derived for the calibration of CW and LFM signals. These results are confirmed by simulated and real data comparisons between line and cardioid array calibrated measurements. This paper is organized as follows: section II describes the triplet arrays, section III presents the general analysis of the cardioid beamformer, IV presents the calibration factors for the specific cases of CW and LFM signals, V includes real and synthetic data calibration examples, VI shows the effects of intra-triplet noise on cardioid beamforming, and VII summarizes the results of this work.

II. Cardioid or triplet arrays

Cardioid or triplet arrays are towed arrays consisting of a line of triplets instead of a line of single hydrophones. Each triplet consists of three closely-spaced omnidirectional hydrophones which are evenly mounted on a circle perpendicular to the array axis. Referenced on the right-handed Cartesian system (X, Y, Z), Y is the array axis pointing at the towing direction, the X axis points at starboard broadside and the Z axis points at the sea surface as shown in Fig. 1. Let K be the number of triplets in the array and let $k = 1, 2, \ldots, K$ be the triplet index. Similarly, let $j = 1, 2, 3$ be the index of the hydrophones within each triplet. The angular separation between the equally-spaced triplet sensors is denoted as γ, where $\gamma = \frac{2}{3}\pi$.

Due to forces applied on the array during the tow, the array is often twisted with regard to its original deployment position. The twist angle of the k-th triplet is denoted as β_k and is defined clockwise with respect to the Z axis. Then the angles of each sensor with respect to Z can be defined as follows:

$$\begin{aligned} \phi_{1k} &= \beta_k \\ \phi_{2k} &= \beta_k + \gamma \\ \phi_{3k} &= \beta_k - \gamma \end{aligned} \tag{1}$$

1-4244-0115-1/06/$20.00 ©2006 IEEE

Report Documentation Page

Form Approved
OMB No. 0704-0188

1. REPORT DATE	2. REPORT TYPE	3. DATES COVERED
01 SEP 2006	**N/A**	**-**

4. TITLE AND SUBTITLE	5a. CONTRACT NUMBER
Unambiguous triplet array beamforming and calibration algorithms to facilitate an environmentally adaptive active sonar concept	5b. GRANT NUMBER
	5c. PROGRAM ELEMENT NUMBER
6. AUTHOR(S)	5d. PROJECT NUMBER
	5e. TASK NUMBER
	5f. WORK UNIT NUMBER
7. PERFORMING ORGANIZATION NAME(S) AND ADDRESS(ES) **NATO Undersea Research Centre Viale S. Bartolomeo 400 La Spezia, Italy**	8. PERFORMING ORGANIZATION REPORT NUMBER
9. SPONSORING/MONITORING AGENCY NAME(S) AND ADDRESS(ES)	10. SPONSOR/MONITOR'S ACRONYM(S)
	11. SPONSOR/MONITOR'S REPORT NUMBER(S)

12. DISTRIBUTION/AVAILABILITY STATEMENT
Approved for public release, distribution unlimited

13. SUPPLEMENTARY NOTES
See also ADM002006. Proceedings of the MTS/IEEE OCEANS 2006 Boston Conference and Exhibition Held in Boston, Massachusetts on September 15-21, 2006, The original document contains color images.

14. ABSTRACT

15. SUBJECT TERMS

16. SECURITY CLASSIFICATION OF:			17. LIMITATION OF ABSTRACT	18. NUMBER OF PAGES	19a. NAME OF RESPONSIBLE PERSON
a. REPORT	b. ABSTRACT	c. THIS PAGE			
unclassified	**unclassified**	**unclassified**	**UU**	**6**	

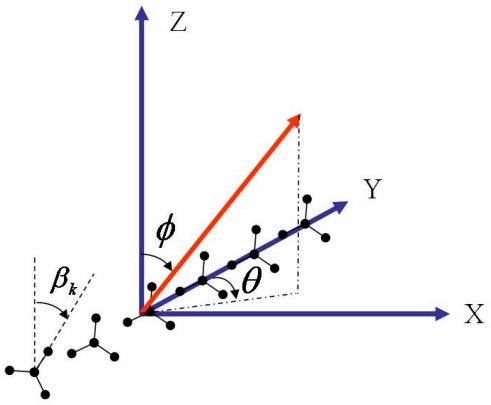

Fig. 1. Sketch of a triplet array referenced in a right-handed Cartesian system.

According to this notation, the vector v_{jk} defining the position of the j-th hydrophone within the k-th triplet is

$$v_{jk} = \begin{bmatrix} r\sin\phi_{jk} \\ y_k \\ r\cos\phi_{jk} \end{bmatrix} \tag{2}$$

where r is the radius of the pitch circle the hydrophones are mounted on and y_k is the Y coordinate of the k-th triplet. From the above expression follows that estimation of the array twist is necessary for correct hydrophone positioning. The twist is usually measured by roll sensors evenly distributed along the array.

III. Cardioid beamforming

Triplet or cardioid arrays are utilized to resolve the port/starboard (left/right) ambiguity problem using a beamforming algorithm, called *cardioid beamforming*. The cardioid beam pattern is derived from the beam pattern of a normal line array [4] weighted by a cardioid-shaped function that places a null at the ambiguous side [5]. The current section describes the time domain derivation of this cardioid beamforming function. The steering direction is defined as (θ, ϕ), where θ is the azimuth angle (clockwise) on the X-Y plane and ϕ is the elevation angle (from vertical) on the X-Z plane (see Fig. 1). Consequently, the unit vector $u(\theta, \phi)$ is defined as

$$u(\theta,\phi) = \begin{bmatrix} \sin\phi\sin\theta \\ \sin\phi\cos\theta \\ \cos\phi \end{bmatrix} \tag{3}$$

The signals received on the triplet phones are related in the following way:

$$s_{jk} = s_k(t - d_{jk}) \tag{4}$$

where

$$d_{jk} = \frac{\langle u(\theta,\phi)\cdot v_{jk}\rangle}{c} \tag{5}$$

is the time delay between the triplet phones defined by the ratio of the projection of v_{jk} on $u(\theta, \phi)$ to the sound speed c, where $\langle\cdot\rangle$ is the scalar operator, i.e the inner product of the two vectors given by the following equation

$$\begin{aligned} \langle u(\theta,\phi)\cdot v_{jk}\rangle \quad = \quad & r(\sin\phi_{jk}\sin\phi\sin\theta + \\ & y_k\sin\phi\cos\theta + \cos\phi_{jk}\cos\phi) \end{aligned} \tag{6}$$

Without loss of generality, it can be assumed that the origin of the reference system and the centre of the triplet coincide and $y_k = 0$, so the inner product can be simplified as follows

$$\langle u(\theta,\phi)\cdot v_{jk}\rangle = r(\sin\phi_{jk}\sin\phi\sin\theta + \cos\phi_{jk}\cos\phi) \tag{7}$$

Cardioid beamforming is implemented by a) shifting the triplet signals to the centre of the triplet, b) weighting them by their projection on a desired direction and c) summing them. The mathematical expression of this algorithm is given by the following formula:

$$b_k(\theta,\phi) = \sum_{j=1}^{3} s_{jk}(t - d_{jk})\,\langle u(\theta,\phi)\cdot v_{j,k}\rangle \tag{8}$$

The main idea of the cardioid beamformer is to suppress the signal arriving from the ambiguous direction. In this case, the signals received on the triplet phones are defined as:

$$s_{jk} = s_k(t + d_{jk}) \tag{9}$$

By substituting this expressions for s_{jk} in (8) the beamformer output on the ambiguous side becomes :

$$b_k(\theta,\phi) = \sum_{j=1}^{3} s_k(t)\,\langle u(\theta,\phi)\cdot v_{j,k}\rangle \tag{10}$$

or equivalently (see Annex 2)

$$b_k(\theta,\phi) = s_k(t)\sum_{j=1}^{3}\langle u(\theta,\phi)\cdot v_{j,k}\rangle = 0 \tag{11}$$

On the other hand, the beamformer output at the steering direction, in which s_{jk} is given by (4), becomes (see Annex 2):

$$b_k(\theta,\phi) = \sum_{j=1}^{3} s_k(t - 2d_{jk})\,\langle u(\theta,\phi)\cdot v_{j,k}\rangle \tag{12}$$

This expression is the output of a single triplet cardioid beamformer in the steering direction of the desired signal. The calibration factor is the relationship between input $s(t)$ and output $b_k(\theta, \phi)$ signals, and is derived in the next section.

IV. Cardioid Calibration

The goal here is to derive an analytical relationship that relates the input and output signals of the cardioid beamformer. Initially this derivation is obtained for a CW and then it is extend to LFM signals.

A. Calibration for CW signals

Let us consider a continuous wave signal of amplitude A and frequency f

$$s(t) = A\cos(2\pi ft) \tag{13}$$

By substituting the CW signal in (12) we obtain (see Annex 2)

$$b_k(\theta,\phi) = A\cos(2\pi ft)b_1 + A\sin(2\pi ft)b_2 \tag{14}$$

where

$$b_1 = \sum_{j=1}^{3}\cos(4\pi f d_{jk})\,\langle u(\theta,\phi)\cdot v_{jk}\rangle \tag{15}$$

and

$$b_2 = \sum_{j=1}^{3}\sin(4\pi f d_{jk})\,\langle u(\theta,\phi)\cdot v_{jk}\rangle \tag{16}$$

The coefficients b_1 and b_2 are plotted as a function of the array roll factor β for different frequency values f. The coefficient b_1 (Fig. 2), demonstrate significant variations with β, especially at high frequencies. On the other hand, b_2 (Fig. 3) is more stable and quasi independent of β at all frequencies (variations are not visible at this scale). It is important to observe that the b_1 values are negligible with respect to b_2 values.The ratios between b_1 and the maximum over β of b_2 are approximately 48dB, 34dB, 28dB and 18dB, for frequencies from 100Hz to 3000Hz. The relationship between

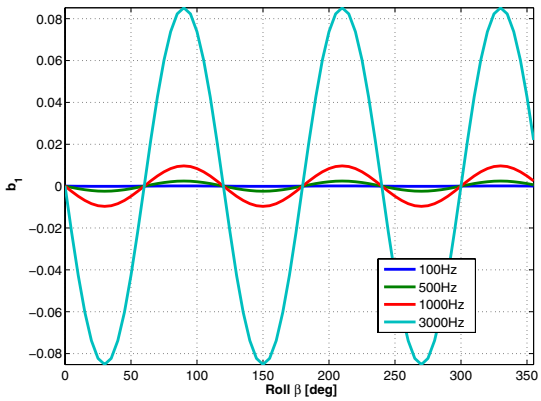

Fig. 2. Coefficient b_1 plotted for $\beta = [0;360]$ and f = [100, 500, 1000, 3000]Hz.

these two coefficients is demonstrated using an example in which the nulling direction is assumed on the horizontal plane, i.e. $\phi = \pi/2$. Then the scalar product becomes:

$$\langle u(\theta,\pi/2)\cdot v_{jk}\rangle = r\sin\phi_{jk}\sin\theta \tag{17}$$

The substitution in b_1 and b_2 gives:

$$b_1 = \sum_{j=1}^{3}\cos(4\pi fr/c\sin\phi_{jk}\sin\theta)r\sin\phi_{jk}\sin\theta \tag{18}$$

and

$$b_2 = \sum_{j=1}^{3}\sin(4\pi fr/c\sin\phi_{jk}\sin\theta)r\sin\phi_{jk}\sin\theta \tag{19}$$

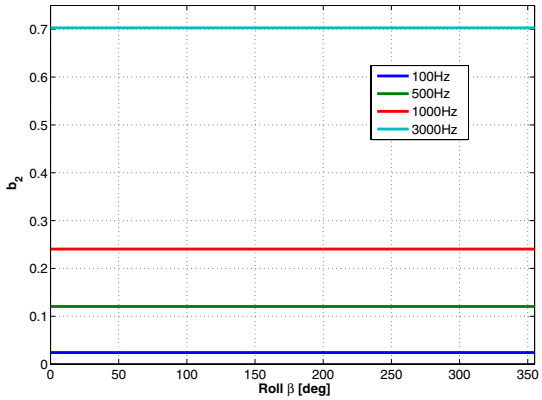

Fig. 3. Coefficient b_2 plotted for $\beta = [0;360]$ and f = [100, 500, 1000, 3000] Hz.

As the radius r of the array is 2 to 2.5cm, for frequencies of the order of a few KHz, the argument of the sinusoidal functions in b_1 and b_2 is $\ll 1$ and therefore can be approximated by the first terms of their Taylor series. The resulting expressions are (see Annex 2)

$$\begin{array}{rcl} b_1 & \approx & -8(\pi f/c)^2(r\sin\theta)^3\sum_{j=1}^{3}\sin^3\phi_{jk} \\ b_2 & \approx & 6\pi f(r\sin\theta)^2/c \end{array} \tag{20}$$

Equations 20 suggest that

$$|b_1| \le -8(\pi f/c)^2(r\sin\theta)^3 = \frac{4\pi fr}{3c}\sin\theta|b_2| \tag{21}$$

thus $|b_1| \ll |b_2|$ for the frequency regime of interest. This relationship is also confirmed by figures 2) and 3). By eliminating the b_1 term, the beamformer's output can be approximated as follows:

$$b_k(\theta,\phi) \approx A\sin(2\pi ft)6\pi f(r\sin\theta)^2/c \tag{22}$$

which indicates that the input/output coefficient for CW pulses is

$$C_{CW} = 6\pi f(r\sin\theta)^2/c \tag{23}$$

and therefore the calibration factor is $1/C_{CW}$.

B. Calibration for frequency modulated signals

The calibration factor derived for a CW signal can still be used in the case of a frequency modulated signal provided that a) the instantaneous frequency is the same for all triplet hydrophones, and b) there is a process that takes into account the time dependence of the instantaneous frequency. Here we examine the validity of these two assumptions for the simple case of an LFM signal.

For an LFM pulse the frequency change associated with time delay d_{jk} is

$$f_{jk} = f_c - \frac{B}{2} + \frac{B}{2T}(t - d_{jk}) \tag{24}$$

where j and k are the hydrophone and the triplex indexes, B is the signal bandwidth, T is the signal duration, and f_c

is the signal central frequency. The instantaneous frequency difference between hydrophones of the same triplet is

$$\begin{aligned} \Delta f_{ijk} &= f_{ik} - f_{jk} \\ &= \tfrac{B}{2T}(d_{jk} - d_{ik}) \end{aligned} \tag{25}$$

By substituting the expressions for the time delay d_{jk} from (1) and (6) the equation is derived

$$\Delta f_{ijk} = \frac{B}{2T}\frac{r}{c}\sin\theta\sin(\beta_k \pm \gamma/2)\sin(\pm\gamma/2) \tag{26}$$

in which $\gamma = \frac{2}{3}\pi$, thus the maximum value of instantaneous frequency difference is

$$\Delta f_{MAX} = \frac{B}{2T}\frac{r}{c}\frac{\sqrt{3}}{2} \tag{27}$$

When $\Delta f_{MAX} \ll 1$, it can be assumed that the instantaneous frequency between triplet phones is the same, i.e.

$$\frac{B}{T} \ll \frac{4c}{\sqrt{3}r} \tag{28}$$

For LFM signals with pulse duration of a few seconds and bandwidth of the order of a couple of KHz, this is true and the calibration formula derived for a CW signal can still be used. The problem is that the calibration factor is frequency dependent. For the special case of an LFM signal, it is found that a single calibration factor that corresponds to the centre frequency of the pulse provides correct results when used in conjunction with a matched filter. This is not a surprising result because the matched filter, by means of integrating the received energy over the entire signal series, averages out the overestimation/underestimation of the calibration factor around the central frequency f_c. So, it can be concluded that $1/C_{LFM}$ may be used for cardioid beamforming calibration of an LFM signal with central frequency f_c, where C_{LFM} is given by the expression

$$C_{LFM} = 6\pi f_c(r\sin\theta)^2/c. \tag{29}$$

This conclusion is verified in the next section using both synthetic and real data.

V. LFM PULSE CALIBRATION EXAMPLES - SIMULATION AND REAL DATA.

A. Simulated data calibration

The cardioid beamforming calibration simulation example presented here is based on a LFM pulse with centre frequency $f_c = 1200$Hz, bandwidth $B = 400$Hz, and duration $T = 1$s. The scenario assumes a point target at 315 degrees and negligible background noise. The received beamformed time series is first calibrated using equation 29 and then matched filtered. The matched filter output is compared with the corresponding result of a line array with a matched 0 dB gain, i.e. the maximum value of the matched filter output corresponds to the amplitude of the signal received. Figure 4 shows the line array response (red line) and the calibrated cardioid array response (blue line) as a function of steering angle. As the two beam patterns are calibrated, the sidelobe levels can be compared directly. The cardioid beamformer has equal or better sidelobe behavior than the line array beamformer, with the exception of the regime near endfire where the calibrated cardioid algorithm demonstrates singularities due to the fact that $C_{LFM} = 0$ for $\theta = (0, \pi)$. In practice, calibrated cardioid processing may be used to about 10 degrees from forward or backward endfire and then be replaced by line array beamforming.

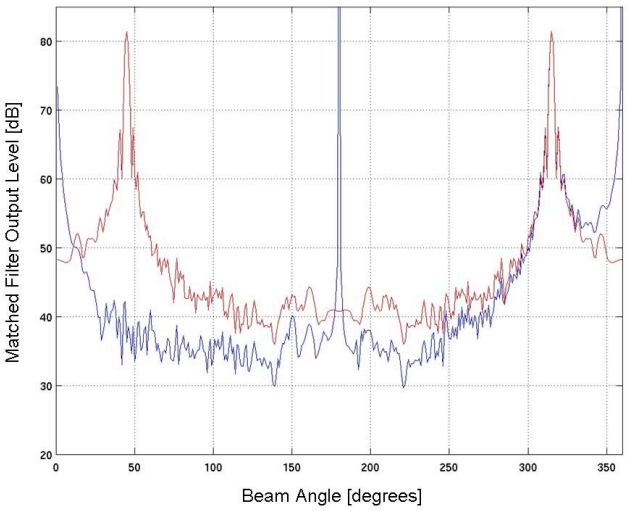

Fig. 4. Comparison of calibrated single line (red) and cardioid (blue) beampatterns after matched filtering using synthetic data.

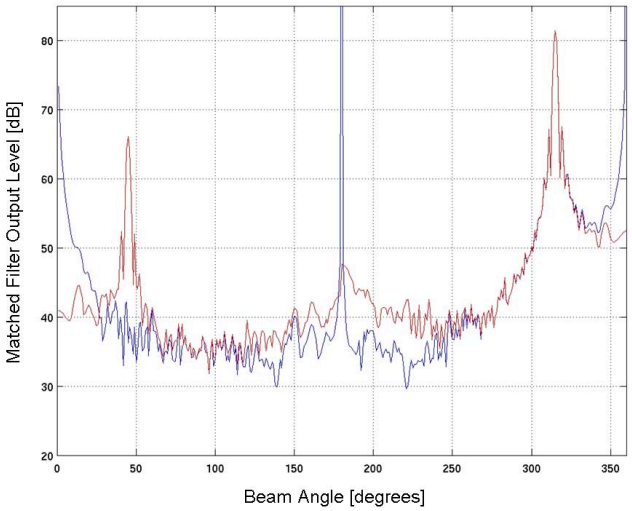

Fig. 5. Comparison of calibrated standard (blue) and modified (red) beampatterns after matched filtering using synthetic data.

An alternative way to address this singularity issue is to modify the cardioid beamformer so that it will have a fixed null at $\theta = \pi/2$. The beampatterns obtained with the two cardioid beamforming algorithms are compared in Fig. 5, where the blue line corresponds to the standard algorithm and the red line corresponds to the modified one. The comparison between the two beampatterns shows that the modified algorithm offers a reduced left-right suppression for a target at 315 degrees, but

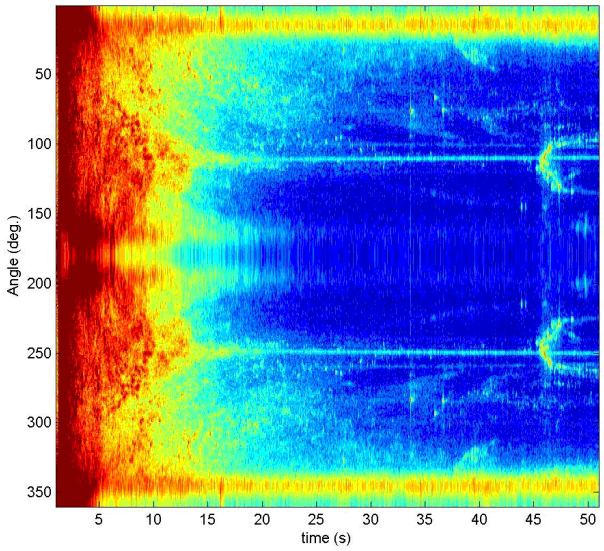

Fig. 6. Matched filter output for single-line array beamforming (no target present).

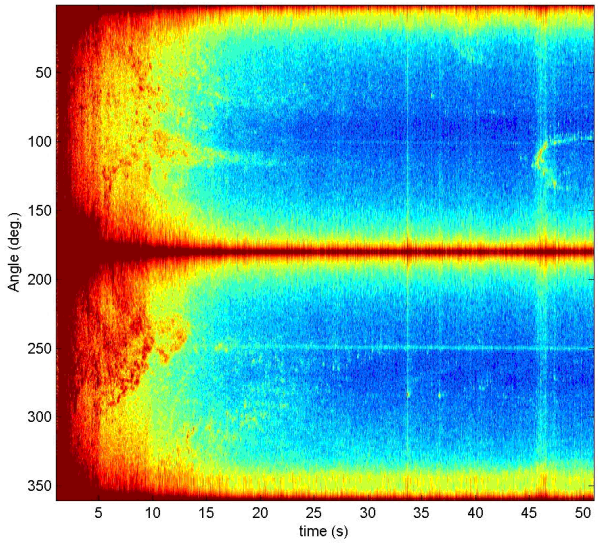

Fig. 7. Matched filter output for standard calibrated cardioid beamforming (no target present).

the endfire singularities are removed.

B. Real data calibration

Calibrated cardioid beamforming was tested also with real data acquired during the BASE'04 sea trial conducted by the NATO Undersea Research Centre [3]. In this section we show the results based a single ping of active sonar data using cardioid beamforming and matched filtering of an LFM pulse with centre frequency $f_c = 1050$Hz, bandwidth $B = 500$Hz and duration $T = 3$s. The calibration results are shown in figures 6-8. The same color scale is used in all images. Figure 6 is the result of line array processing and is symmetric around 180 degrees. Figure 7 shows the results for the standard calibrated cardioid algorithm and the known problems at forward

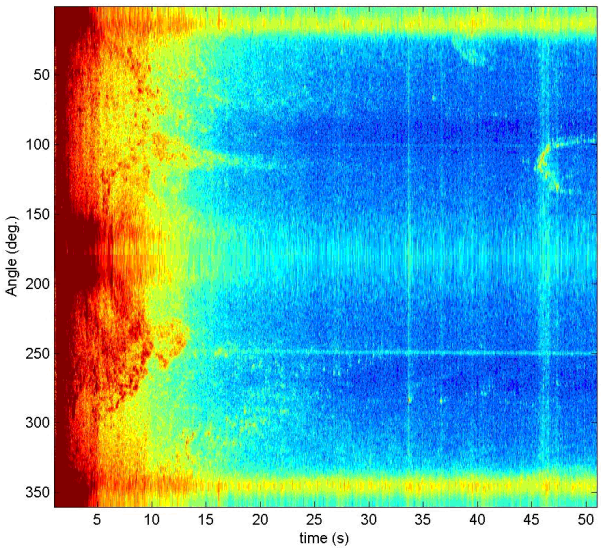

Fig. 8. Matched filter output for modified calibrated cardioid beamforming (no target present).

and backward endfire can be observed easily. Figure 8 is the result for the modified cardioid algorithm. The comparison between line and cardioid processing validates the suggested LFM calibration process. The comparison between the two cardioid beamforming algorithms demonstrates the elimination of endfire singularities in the case of the standard algorithm. More information regarding the derivation of the modified calibrated cardioid beamforming and its pros and cons with respect to the standard algorithm can be found in [5].

VI. The effect of intra-triplet noise

Due to the small intra-triplet distances, the noise between triplet phones is usually highly correlated. However electric noise or flow noise due to high towing speed may generate uncorrelated noise between triplet phones. Intra-triplet noise correlation, which affects considerably the output of the cardioid beamformer, is also addressed in [6]. This is shown in Fig. 9 where the matched filter output of a simulated point target at broadside is shown for three cases: cardioid beamforming assuming correlated intra-triplet noise (red), conventional line array beamforming (blue) and cardioid beamforming assuming uncorrelated intra-triplet noise (green). The comparison between cardioid and conventional line array processing shows that, for the same detection output at the target location, the noise level after cardioid beamforming is much lower. However, in the case where the intra-triplet noise is uncorrelated, the interference level after cardioid beamforming becomes so high that the target is no longer detectable, and therefore directional beamforming is no more relevant.

VII. Conclusions

Analytical expressions for the calibration of cardioid beamforming are derived for CW and LFM signals. The calibration factor was found to be frequency dependent. In the LFM case,

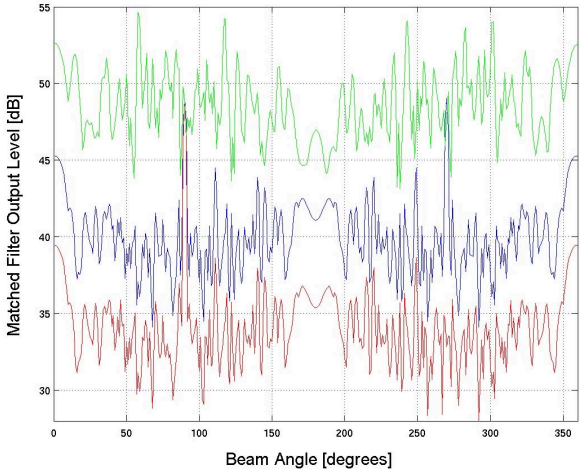

Fig. 9. Matched filter output results for a simulated point target at broadside. Three beamforming cases are compared: a) cardioid beamforming with intra-triplet correlated noise (red), cardioid beamforming with intra-triplet uncorrelated noise (green), standard line array beamforming (blue).

it was shown that calibration can be approximated using the pulse central frequency as the matched filter detector, which is applied after beamforming, averages out the calibration offset due to frequency mismatch. The validity of the mathematical expressions was demonstrated using simulated and real data analysis. A comparison between the standard beamformer and a modified version designed to suppress endfire singularities is also shown. The degradation of cardioid beamforming in the case of uncorrelated intra-triplet noise was also demonstrated using a simulated scenario with a point target. These results will be utilized in an active adaptation scheme to provide system feedback based on real life comparisons between real and synthetic data. The next step in the analysis is to generalize the calibration derivation for a broader category of frequency modulated pulses.

ACKNOWLEDGMENTS

The content of this document pertains to work performed under Project 04C3 of the NATO Undersea Research Centre Scientific Programme of Work. The BASE '04 data set is part of the BASE '04 Joint Research Project, a collaboration between NATO Undersea Research Centre and Defence Research and Development Canada - Atlantic.

ANNEX 1: USEFUL TRIGONOMETRIC EXPRESSIONS

In the derivation of the cardioid beamformer response we often have to deal with expressions which are sum of three trigonometric functions with arguments ϕ_{jk}. If we substitute to ϕ_{jk} the values in (1), where $\gamma = \frac{2}{3}\pi$, we obtain the following equivalences which are satisfied $\forall\beta$:

$$\begin{aligned}
&\sin\beta + \sin(\beta+\gamma) + \sin(\beta-\gamma) = 0\\
&\cos\beta + \cos(\beta+\gamma) + \cos(\beta-\gamma) = 0\\
&\sin^2(\beta) + \sin^2(\beta+\gamma) + \sin^2(\beta-\gamma) = 3/2\\
&\cos^2(\beta) + \cos^2(\beta+\gamma) + \cos^2(\beta-\gamma) = 3/2
\end{aligned} \tag{30}$$

ANNEX 2: DERIVATION OF RESULTS

Derivation of (11)

$$\begin{aligned}
b_k(\theta,\phi) &= \textstyle\sum_{j=1}^{3} s_{jk}(t-d_{jk})\,\langle u(\theta,\phi)\cdot v_{j,k}\rangle\\
&= \textstyle\sum_{j=1}^{3} s_k(t+d_{jk}-d_{jk})\,\langle u(\theta,\phi)\cdot v_{j,k}\rangle\\
&= \textstyle\sum_{j=1}^{3} s_k(t)\,\langle u(\theta,\phi)\cdot v_{j,k}\rangle\\
&= s_k(t) r\big[\sin\phi\sin\theta\textstyle\sum_{j=1}^{3}\sin\phi_{jk} +\\
&\quad \cos\phi\textstyle\sum_{j=1}^{3}\cos\phi_{jk}\big]\\
&= 0
\end{aligned} \tag{31}$$

where the second and third equations in Annex 1 are also used.

Derivation of (12)

$$\begin{aligned}
b_k(\theta,\phi) &= \textstyle\sum_{j=1}^{3} s_{jk}(t-d_{jk})\,\langle u(\theta,\phi)\cdot v_{j,k}\rangle\\
&= \textstyle\sum_{j=1}^{3} s_k(t-d_{jk}-d_{jk})\,\langle u(\theta,\phi)\cdot v_{j,k}\rangle\\
&= \textstyle\sum_{j=1}^{3} s_k(t-2d_{jk})\,\langle u(\theta,\phi)\cdot v_{j,k}\rangle
\end{aligned} \tag{32}$$

Derivation of (14)

$$\begin{aligned}
b_k(\theta,\phi) &= \textstyle\sum_{j=1}^{3} A\cos((2\pi f(t-2d_{jk})))\,\langle u(\theta,\phi)\cdot v_{j,k}\rangle\\
&= A\textstyle\sum_{j=1}^{3}\cos(2\pi ft)\cos(4\pi f d_{jk})\,\langle u(\theta,\phi)\cdot v_{j,k}\rangle +\\
&\quad A\textstyle\sum_{j=1}^{3}\sin(2\pi ft)\sin(4\pi f d_{jk})\,\langle u(\theta,\phi)\cdot v_{j,k}\rangle\\
&= A\cos(2\pi ft)\textstyle\sum_{j=1}^{3}\cos(4\pi f d_{jk})\,\langle u(\theta,\phi)\cdot v_{j,k}\rangle +\\
&\quad A\sin(2\pi ft)\textstyle\sum_{j=1}^{3}\sin(4\pi f d_{jk})\,\langle u(\theta,\phi)\cdot v_{j,k}\rangle\\
&= A\cos(2\pi ft)b_1 + A\sin(2\pi ft)b_2
\end{aligned} \tag{33}$$

Derivation of (20)

By using the truncated Taylor expansion we can approximate sin and cos with small arguments as:

$$\begin{aligned}
\sin\epsilon &\approx \epsilon\\
\cos\epsilon &\approx 1-\epsilon^2/2
\end{aligned} \tag{34}$$

By substituting the approximations in (18), (19) we obtain:

$$\begin{aligned}
b_1 &\approx \textstyle\sum_{j=1}^{3}\big(1-1/2\big(4\pi fr/c\sin\phi_{jk}\sin\theta\big)^2\big) r\sin\phi_{jk}\sin\theta\\
&= r\sin\theta\textstyle\sum_{j=1}^{3}\sin\phi_{jk} - 8(\pi f/c)^2(r\sin\theta)^3\textstyle\sum_{j=1}^{3}\sin^3\phi_{jk}\\
&= -8(\pi f/c)^2(r\sin\theta)^3\textstyle\sum_{j=1}^{3}\sin^3\phi_{jk}
\end{aligned} \tag{35}$$

and

$$\begin{aligned}
b_2 &\approx \textstyle\sum_{j=1}^{3} 4\pi fr/c\sin\phi_{jk}\sin\theta r\sin\phi_{jk}\sin\theta\\
&= 4\pi f(r\sin\theta)^2/c\textstyle\sum_{j=1}^{3}\sin^2\phi_{jk}\\
&= 6\pi f/c(r\sin\theta)^2
\end{aligned} \tag{36}$$

REFERENCES

[1] R. J. Urick, *Principles of Underwater Sound*. McGraw-Hill, New York, 1983.
[2] A. D. Waite, *SONAR for Practising Engineers*. Wiley, UK, 2002.
[3] G. Haralabus, A. Baldacci, R. Laterveer, M. van Velzen, *Broadband active detection in reverberation-limited conditions*, Proc. of ECUA 2004, Delft, The Netherlands, July 2004.
[4] S. Haykin, *Array signal processing*. Prentice-Hall, 1985.
[5] D. T. Hughes, *Aspects of cardioid processing*, SACLANTCEN SR-329, 2000.
[6] M. van Velzen, G. Haralabus, A. Baldacci, *Calibration of Cardioid Beamforming Algorithms*, NURC SR-435, 2005.